



Organic carbon in a seepage face of a subterranean estuary: Turnover and microbial interrelations

Shan Jiang^{a,*}, Yixue Zhang^a, Jie Jin^a, Ying Wu^a, Yongjun Wei^b, Xiaolu Wang^a, Carlos Rocha^c, Juan Severino Pino Ibánhez^{c,d}, Jing Zhang^{a,e}

^a State Key Laboratory of Estuarine and Coastal Research, East China Normal University, Shanghai 200062, China

^b School of Pharmaceutical Sciences, Key Laboratory of State Ministry of Education, Key Laboratory of Henan province for Drug Quality Control and Evaluation, Collaborative Innovation Center of New Drug Research and Safety Evaluation, Zhengzhou University, Zhengzhou, Henan 450001, China

^c Biogeochemistry Research Group, School of Natural Sciences, Trinity College Dublin, Dublin 2, Ireland

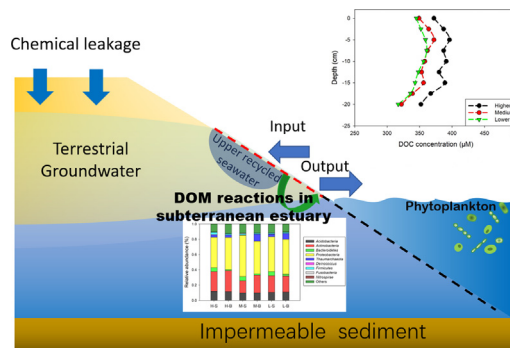
^d Instituto de Investigaciones Mariñas, Consejo Superior de Investigaciones Científicas (IIM-CSIC), Eduardo Cabello 6, 36208 Vigo, Spain

^e School of Oceanography, Shanghai Jiao Tong University, Shanghai 200040, China

HIGHLIGHTS

- Production and removal of DOC in a seepage face in the Sanggou Bay were obtained.
- DOC production was mainly driven by decomposition of SOC via heterotrophic microbes.
- DOC removal was found in the surface layer, mainly linked to biological assimilation.
- Changes of sediment microbial community structure may influence DOC turnover rates.
- Porewater temperature and flow rates also impacted DOC reaction rates.

GRAPHICAL ABSTRACT



ARTICLE INFO

Article history:

Received 22 December 2019

Received in revised form 2 March 2020

Accepted 24 March 2020

Available online 25 March 2020

Editor: José Virgílio Cruz

Keywords:

Microbiota
Organic carbon
Remineralization
Seepage face
Seasonal variation
Subterranean estuaries

ABSTRACT

Subterranean estuaries, the mixing zone between terrestrial groundwater and coastal seawater, are important biogeochemical hotspots. In the present study, organic carbon cycling and related drivers, including the characterization of different organic carbon pools and sediment microbial community, were investigated in a subterranean estuary seepage face. Within the first 20 cm depth seepage face sediments, both production and removal of dissolved organic carbon (DOC) were observed, mainly driven by heterotrophic microbes. From spring to autumn, active DOC production occurred on the seepage face at the 15–20 cm depth, likely via aerobic degradation of sediment organic carbon (SOC) with subsequent release of dissolved fractions into the porewater. During winter, DOC production moved to a shallower depth of the seepage face due to increasing SOC content in the surface layer. DOC production rate depended on heterotrophic microbial biomass (e.g. *Proteobacteria*) and was enhanced by high microbial activity and porewater advection. DOC removal frequently occurred at the 0–5 cm depth layer except in winter. The seasonal shift in carbon source utilization (SOC to DOC) in this layer likely resulted from the decrease in SOC pool, especially the labile portion of SOC and the increased availability of DOC due to production in the deeper sediment (15–20 cm). Given the similarity in microbial community structure along the sediment profile, this shift suggests SOC as the preferential carbon source for benthic microbes as well as adaptive flexibility

* Corresponding author.

E-mail address: sjiang@sklec.ecnu.edu.cn (S. Jiang).

in microbial carbon source utilization. DOC removal was also significantly tied to microbial activity and advection rate. Because DOC production rates were higher compared to DOC consumption the seepage face acted as a net source of DOC to the coastal ecosystem.

© 2020 Elsevier B.V. All rights reserved.

1. Introduction

The coastal zone is the locus of interaction between terrestrial and marine ecosystems. Approximately 0.5 Pg C yr^{-1} of terrestrial organic matter is delivered to the coastal ocean via continental surface loading (Bianchi, 2011). It is estimated that 30% of that amount is buried annually in coastal sediments (Bianchi, 2011), while the majority of the remaining fraction is consumed in coastal environments via a wide range of biogeochemical reactions, e.g. photobleaching, aerobic/anaerobic respiration, biological assimilation (Cebrian, 2002). Coastal zones are also subject to increasing human occupancy, and presently host >50% of the global population (Small and Nicholls, 2003). Coastal seas receive substantial amounts of terrestrial solutes derived from human activities via surface loadings, atmospheric deposition and submarine groundwater discharge (SGD; Moore, 2010). The significant contribution of land-borne nutrient and trace metals boosts primary productivity of coastal seas and despite low global surface area, coastal primary productivity accounts for >20% of net oceanic primary productivity (Probandt et al., 2017). This enhanced primary production node also accelerates carbon-dependent reactions. Currently, carbon turnover in coastal belts is acknowledged to be a major component of global carbon cycles and budgets (Bauer et al., 2013). Nevertheless, the fate of different forms of carbon in coastal settings is poorly understood (Bauer et al., 2013), mainly due to relatively limited observation sets, but also to a complex network of highly variable environmental factors and drivers.

Generally, coastal sediments can be divided into cohesive (muddy) and permeable (sandy) sediments according to grain size and permeability (Huettel et al., 2014). Cohesive sediments occupy approximately 40% of the global coastal shorelines. Given their high carbon sequestration capability, a large inventory of organic carbon is frequently recorded in cohesive sediments (e.g. fjord sediments: Smith et al., 2015; mangrove sediments: Jiang et al., 2017; estuarine sediments: Wu et al., 2019). Accordingly, carbon-dependent reactions in cohesive sediments are generally assumed to be highly active (Huettel et al., 2014). In contrast with cohesive sediments, permeable sediments evidence low carbon storage, frequently below the level of 0.1% by weight (e.g. Ibánhez and Rocha, 2016). However, permeable sediments play a key role in carbon cycling (Rocha, 2008; Huettel et al., 2014). Specifically, diffusion is the dominant pathway for solute transport in cohesive sediments, while advection, driven by thermal convection, gravity waves, inland pressure head, Bernoulli effects and tidal pumping, is the main path for the solute transport in permeable sediments (Boudreau et al., 2001). Compared with diffusion, the transport efficiency caused by advection is frequently 2 to 3 orders of magnitude higher (Huettel et al., 1998; Rocha, 1998; Moore, 1999). The rapid delivery of reactants combined with fast removal of reaction products support high benthic reaction rates in permeable sediments and therefore, these are now known to be a 'fast lane' in carbon cycling (Rocha, 2008; Chipman et al., 2010; Seidel et al., 2015; Ibánhez and Rocha, 2016).

Near the littoral zone, subterranean estuaries (STEs) are the mixing region of terrestrial groundwater and coastal seawater (Moore, 1999). The interaction between water with contrasting ionic strengths in this permeable zone makes STEs a node for the processing of both land-derived and pelagic carbon (Couturier et al., 2016), likely mediated by a wide range of microbes, e.g. *Proteobacteria* (*Gamma-*, *Delta-*, *Alpha-*) and *Actinobacteria* (Schöttner et al., 2011; Marchant et al., 2017). The multiple drivers of porewater movement in permeable sediments

accelerate water mixing and enhance reaction rates. In addition, regular exposure to the atmosphere due to tidal phase variation introduces dissolved oxygen (DO) into the intertidal area of STEs, thus feeding aerobic reactions (Charbonnier et al., 2013; Ibánhez and Rocha, 2016). Carbon turnover in STEs is expected to be rapid because of the additive influence of all active enhancing factors focused in one location. Notwithstanding its importance, knowledge gaps in the carbon cycling in STEs still exist, particularly on its seasonality, the impact of environmental drivers and of the dynamic linkage between the benthic microbial community and carbon reactions. These gaps may hamper the understanding of carbon cycling in coastal zones as one of the most active carbon processors in the Earth system. In the present study, seasonal field campaigns were conducted at a seepage face, the outer region of STEs. The research aimed to address the following points: (1) seasonal variation of carbon turnover intensity in the seepage face; (2) potential linkage between sediment microbial community and organic carbon turnover in the seepage face; (3) the response of organic carbon processing and storage to terrestrial/pelagic inputs.

2. Materials and methods

2.1. Sampling site

The sampling site is located at a beach in the Sanggou Bay National Park, Rongcheng City, Shandong Province, China (Fig. 1A). The beach is far away from docks and places of interest recreational, receiving low human interference. The sandy beach, composed of highly permeable sands, delineates the inner coastline of the bay with a length of approximately 7.5 km. The mean depth of Sanggou Bay is 7.5 m and the water surface area reaches 144 km^2 (Zhu et al., 2017). The tidal range of the sampling beach varies from 2 m (spring) to 0.8 m (neap) with a typical semi-diurnal pattern, producing an intertidal area of 20 km^2 (Shi et al., 2013). Coupled with tidal variation, the bay water is intensively exchanged with the Yellow sea via the 11.5 km bay outlet (Wang et al., 2014; Jiang et al., 2015). Water temperature within the bay ranges from 1.6 to 25.6 °C, with the extreme values frequently recorded during February and August, respectively (Yang et al., 2005). The precipitation is approximately 820 mm yr^{-1} , and the main rainy period lasts from May to September.

Sanggou Bay is an important location for fishery and aquaculture (Jiang et al., 2015; Fang et al., 2016), especially kelp (*Laminaria laminaria*), pacific oyster (*Crassostrea gigas*) and scallops (*Chlamys farreri*). The economic benefit of the aquaculture products ranges from 13.2 to 25.2 million Yuan (RMB) $\text{km}^{-1} \text{ yr}^{-1}$ (Shi et al., 2013). Diatoms dominate phytoplankton populations in Sanggou Bay, especially *Paralia sulcata* and *Coscinodiscus oculus-iridis* (Yuan et al., 2014). In summer, the biomass of dinoflagellates significantly increases. The maximum cell abundance of phytoplankton is found in August (average $8.1 \times 10^3 \text{ cells L}^{-1}$) whereas minima are observed in October (average $2.6 \times 10^3 \text{ cells L}^{-1}$; Yuan et al., 2014). Four rivers discharge into Sanggou Bay: the Sanggan River, the Yetao River, the Gu River, and the Xiaoluo River. The Gu River presents the highest discharge rate of all, ranging from 1.7×10^8 to $2.3 \times 10^8 \text{ m}^3 \text{ yr}^{-1}$ (Wang et al., 2014). Apart from the Gu River, SGD, fed from the adjacent coastal aquifers (Hou et al., 2016), is also important for the transport of terrestrial solutes (Wang et al., 2014). Based on radium isotope data, the hot spot for SGD occurs at the inner side of the bay (Wang et al., 2014).

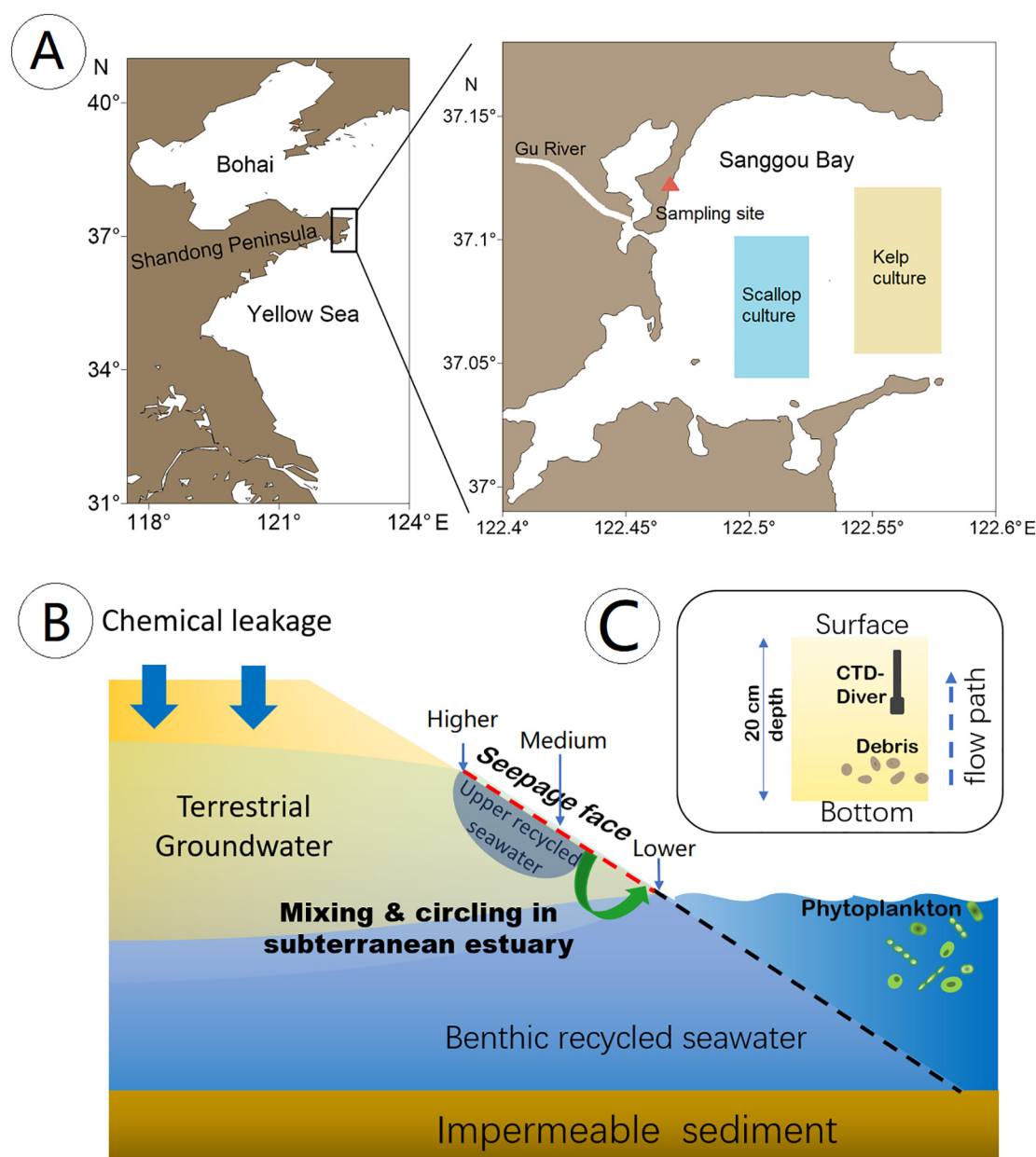


Fig. 1. Location of Sanggou Bay (A). It highlights the location of the sampling beach in the Sanggou Bay and the main regions for the culture of scallop and kelp in the bay. It also shows the location of Gu River, i.e. the largest river to the Sanggou Bay system. This figure is adapted from Zhu et al. (2017); The sketch of the sampling beach (B), which highlights three sampling sites in the seepage face: higher intertidal station; medium intertidal station and lower intertidal station; the sampling depth (20 cm) and location of the buried CTD Diver is outlined in (C).

2.2. Sample collection

Sampling surveys were conducted in April 2018 (Spring), June 2018 (Summer), October 2018 (Autumn) and February 2019 (Winter). All the sampling events were conducted during spring tides to eliminate the influence of tidal variation on porewater outflow rates (Rocha et al., 2009). Wave heights during the sampling events were 20–30 cm. The surveys were conducted at the beach seepage face, in three stations, located respectively in the higher intertidal, lower intertidal and at a mid-point on the intertidal profile (outlined in Fig. 1B).

The distance from the higher intertidal station to the lower intertidal station was approximately 15 m. During each sampling, porewater was extracted with an in-situ profiler based on the design of Ibáñez et al. (2011). The porewater profiler extended from the sediment surface (0 cm) to 20 cm depth (Fig. 1C), and contained 9 sampling ports in total (separated 2.5 cm from each other). At each depth, porewater

was extracted, immediately filtered and stored in acid pre-washed bottles (60 mL). DOC samples were filtered with in-line syringe nylon filters (0.45 μm pore size) while samples for CDOM (colored dissolved organic matter)/FDOM (fluorescent dissolved organic matter) were filtered through polyethersulfone membrane filters (0.22 μm pore size). A small fraction of the filtrates was used for the determination of salinity in the laboratory (Multi 350i probe, WTW, Germany). The filtered samples were stored in pre-combusted amber glass bottles prior to laboratory analyses. Subsequently, porewater at 20 cm depth and 2 cm depth was extracted for DO measurements using a portable probe. Coupled with the porewater collection, a CTD-Diver (van Essen Instruments, The Netherlands) was buried into the sand at a depth of 10 cm (Fig. 1C), recording water pressure and temperature every 30 s during the sampling period.

After porewater collection, a sediment column (approximately 22 cm length) near the extraction site was collected via a sediment

Table 1
Physic-chemical characters of seawater collected at high tide and Gu river water.

	High tide seawater				Gu river water	
	Spring	Summer	Autumn	Winter	Summer	Winter
Salinity	34.2	34.1	34.5	34.5	0	0
Temp. (°C)	16.5	27.4	18.9	4.6	27.6	4.8
DO (%)	100.2	102.5	96.8	99.7	93.2	96.7
Chlorophyll <i>a</i> (µg L ⁻¹)	4.11	4.86	3.24	3.58	–	–
DOC (µM)	145	133	148	137	289	345
α ₃₅₅	0.87	0.79	0.82	0.82	1.68	1.52
S _{275–295}	35.2	34.6	35.3	36.7	24.9	23.6
Amino acid (R.U.)	0.11	0.09	0.12	0.11	0.14	0.12
Amino acid (R.U.)	0.08	0.08	0.09	0.08	0.12	0.11
Terrestrial humic (R.U.)	0.07	0.09	0.09	0.10	0.21	0.20
Bacterial humic (R.U.)	0.06	0.07	0.07	0.08	0.16	0.14

corer. After removing the top layer (approximately 1 cm) to avoid shell debris, the sediment column was sliced into five sections, 1–4, 5–8, 9–12, 13–16 and 17–20 cm depth. The sediment slices were placed into sterilized bags and kept at –20 °C until analysis. During the sampling events, seawater was collected on-site during high tides. Following the same procedure as for porewater samples, seawater DOC and CDOM/FDOM samples were collected. Moreover, seawater aliquots were filtered with pre-combusted GF/F filters (Whatman®, mean pore size: 0.7 µm) to determine chlorophyll *a* concentration. In summer and winter campaigns, water from the Gu River has also collected for DOC and CDOM/FDOM measurements.

2.3. Water sample analyses

DOC was determined in thawed water samples by high-temperature catalytic combustion using a Shimadzu TOC-LCPH total organic carbon analyzer (TOC-LCPH, Shimadzu, Japan) with an ASI-L autosampler. Prior to injection, samples were acidified with 2 M HCL and purged with CO₂-free oxygen to remove inorganic carbon. During the analyses, deep-sea water supplied by the University of Miami (provide by Dr. Hansell) was used as reference to ensure equipment consistency (approximately 4.2%). CDOM analyses were conducted on a spectrophotometer (PERSEE®, China, TU-1901) under the double channel mode. Deionized water purified with a Rephile® gradient system (resistivity: 18.2 mΩ·cm) was used as blank. The scanning wavelength ranged from 250 to 750 nm with 1 nm intervals. The concentration of CDOM in the tested water samples was estimated by the absorption coefficient at 355 nm (Zhang et al., 2009):

$$\alpha_{CDOM}^{355} = 2.303 \times \left(OD_{CDOM}^{355} - OD_{CDOM}^{700} \times \frac{355}{700} \right), \quad (1)$$

where α_{CDOM}³⁵⁵ is the absorption coefficient at 355 nm, OD_{CDOM}³⁵⁵ and OD_{CDOM}⁷⁰⁰ are optical readings at 355 nm and 700 nm, respectively. In addition, the exponential spectral slope was estimated as:

$$\alpha_{CDOM}^m = \alpha_{CDOM}^n \exp(S(n-m)), \quad (2)$$

where α_{CDOM}^m is the absorption coefficient at 'm' nm wavelength, α_{CDOM}ⁿ is the adsorption coefficient at 'n' nm wavelength and S is the exponential spectral slope between n and m nm wavelengths estimated through

linear regression. In the present study, the spectral slope (S_{275–295}) of the wavelength range 275 to 295 nm was calculated (i. e. 295 ≥ m > n ≥ 275). Generally, a large gradient indicates a small molecular weight of the CDOM, likely to be marine-derived solutes. In contrast, a small gradient indicates a large molecular weight, which was frequently characterized as terrestrial material (Zhang et al., 2009). FDOM analyses for all porewater and seawater samples were conducted on a fluorescence spectrometer (Hitachi F-4500) using 3-D matrix scanning. The excitation wavelengths ranged from 250 to 500 nm, while the emission wavelengths ranged from 270 to 550 nm. The wavelength intervals for excitation and emission were 5 nm and 2 nm, respectively. After subtracting the blank (deionized water), the scanned data from the water samples were divided by the integration of the water Raman peak. Then, the unified data were analyzed through the PARAFAC modeling using the FDOM toolbox (Stedmon and Bro, 2008). The PARAFAC modeling results were validated by the split-half analysis function in the toolbox.

2.4. Sediment physico-chemical analyses

A fraction of the sliced sediment samples was dried at 60 °C. The difference between dry weight and initial weight was used in the quantification of sediment porosity following Jiang et al. (2018). The dry samples were used to determine particle size and sediment organic carbon (SOC). Specifically, the grain size was measured directly from sediment subsamples using a Coulter LS 100Q (Coulter Company, USA). The sediment grain size distribution was described as the proportions of clay (<4 µm), silt (4–63 µm), and sand (>63 µm) in each sample. Concentrations of sediment organic carbon (SOC) were analyzed using a CHNOS Elemental Analyzer (Vario EL III) with a relative precision of ±5%. The weight percentage of organic carbon in the sediment samples was analyzed after removing the carbonate fraction with 1 M hydrochloric acid acidification during 24 h (Wu et al., 2019). Hydraulic conductivity was determined according to Rocha et al. (2005). Approximately 1 g of fresh sediment samples were used to quantify chlorophyll *a* content based on the 90% acetone cold extraction (4 °C in a fridge), with airtight non-additive vacutainers (Jiang et al., 2017). The absorbance of the extracted solutes at 665 nm was used to calculate the concentration of sediment chlorophyll *a* (unit: µg g⁻¹ dry sediment; Castle et al., 2011). Chlorophyll *a* content in the filtered GF/F filters were determined with the same analytical approach. In addition, exchangeable organic carbon (EOC) on the sediment particle surface was extracted with 0.5 M potassium chloride solution (12 h). DOC and CDOM/FDOM in the extraction solution were then quantified following the methods aforementioned.

2.5. Benthic microbiota

The microbial activity of the sliced sediment was quantified as the fluorescein diacetate (FDA) hydrolysis potential according to Jiang et al. (2016) based on the tight linkage between hydrolysis reactions and organic matter decomposition (Bianchi, 2011). The hydrolysis potential of the sediment was determined via incubation of 1 g fresh sediment with 200 µg FDA in phosphors buffer solution (pH = 7.3) for 1 h. The reaction was terminated with acetone and the hydrolyzed FDA in the solution was quantified spectrophotometrically at 490 nm.

For characterization of the benthic microbiota, total DNA was extracted from approximately 0.3 g fresh sediment taken from the surface

Table 2
Porewater salinity (mean values from each profile), pressure head (cm), and calculated discharge rate (cm h⁻¹) in different sampling sites in the seepage face among four seasons.

	Salinity			Pressure Head			Discharge rate		
	Higher	Medium	Lower	Higher	Medium	Lower	Higher	Medium	Lower
Spring	34.1	33.1	31.5	3.5	7.2	5.9	9.0	18.4	15.3
Summer	32.4	31.9	31.2	6.3	10.9	8.9	16.1	28.3	22.8
Autumn	33.9	32.8	32.6	2.7	7.8	7.3	4.2	20.2	18.7
Winter	34.2	34.0	33.5	2.9	6.5	5.7	7.1	16.8	14.5

(2 cm depth) and bottom (17 cm) parts of the profile. Subsequently, the V3-V4 regions of microbial 16S rRNA genes in the extracted DNA were amplified. The PCR fragments were then extracted with 2% agarose gels, purified and quantified. The KAPA Hyper Prep Kit (Roche) was used for the 16S rDNA gene amplicon library construction. The library was paired-end sequenced (2×300 bp) on an Illumina Miseq system.

The obtained fastq files were demultiplexed with the barcode sequences adapted to the primers. After removing low-quality (score < 5) 4 bp or shorter than 150 bp reads, USEARCH fastq_mergepairs command (version 9.2.64) with the default parameters was used to merge the paired-end reads (Edgar and Flyvbjerg, 2015). The primer sequences in the merged reads were trimmed. The Operational Taxonomic Units (OTUs) were clustered at 97% identity cutoff with

USEARCH UPARSE. The chimeric sequences were abandoned based on the UPARSE pipeline analysis (Edgar, 2013). The USEARCH SINTAX algorithm was used to analyze phylogenetic affiliation of the obtained 16S rRNA gene sequences with the RDP training set (version v16) 16S rRNA database as the reference and 0.8 as the confidence threshold (Edgar, 2016). The data were deposited into Sequence Read Archive (SRA) of the NCBI database with the accession numbers of SRX7825210-SRX7825233.

2.6. Mathematical calculations

Discharge rate (cm h^{-1}) at each sampling station, identified as the advection rate, was estimated according to Darcy's law as following

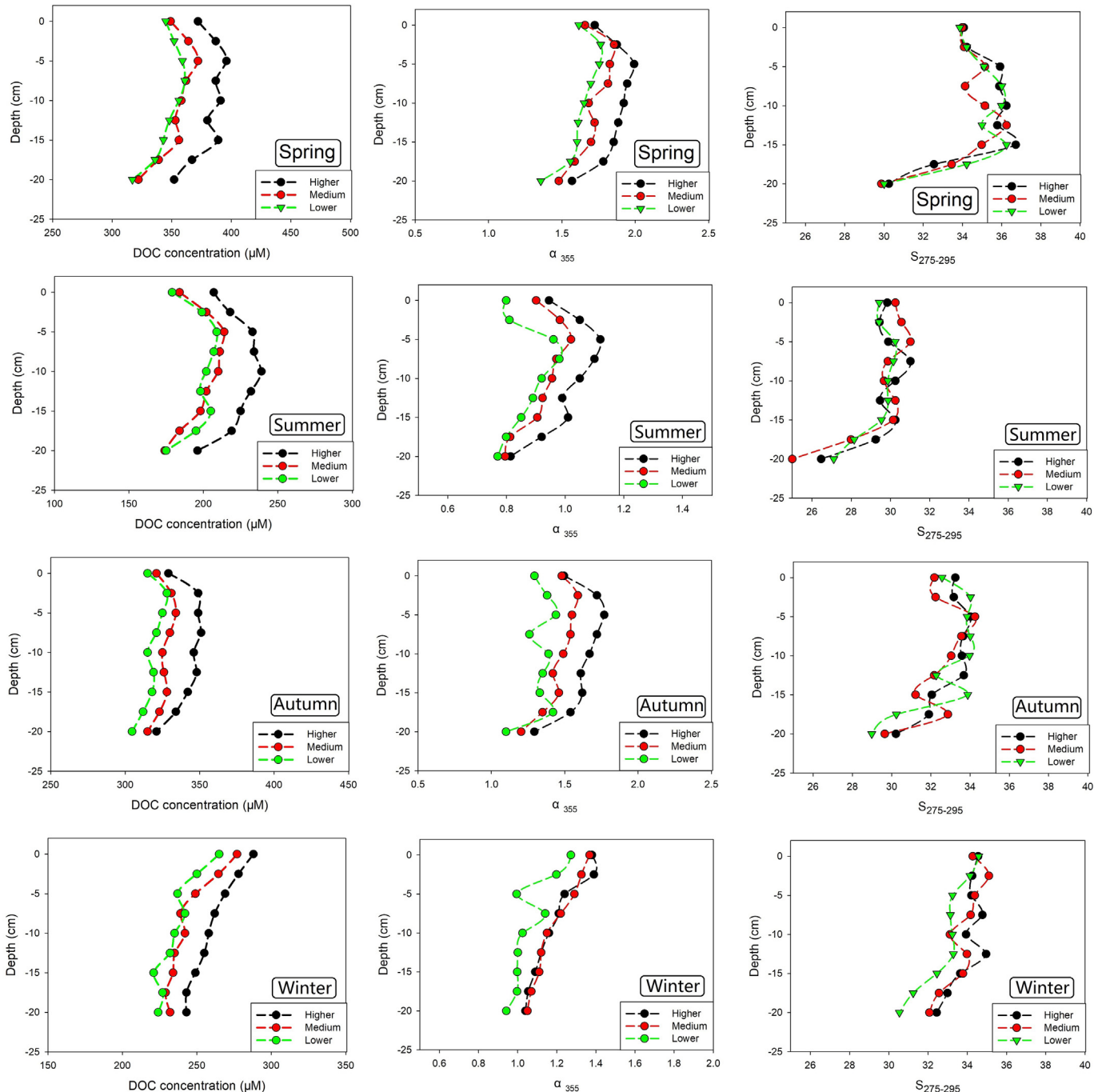


Fig. 2. DOC concentration, α_{355} and $S_{275-295}$ in the porewater profile from three zones (higher, medium and lower) in the seepage face among four seasons.

(Ma et al., 2015):

$$q = \delta K_v \left(\frac{P_{\text{water}} - P_{\text{atm}} - L}{L} - \varepsilon C_s \right), \quad (3)$$

where q is the discharge rate, K_v is the hydraulic conductivity, P_{water} and P_{atm} are the pressure of porewater and atmosphere in the sampling site, expressed in cm of the water column. L is the distance between the sensor and the sediment surface (10 cm here). The term ' $P_{\text{water}} - P_{\text{atm}} - L$ ' defines the hydraulic head. δ , ε and C_s are constants. δ is 0.955, ε is 7.143×10^{-4} and C_s is 28.7 (Ma et al., 2015). With advection rates, reaction rates of DOC and DO along the sampled vertical profiles can be calculated according to a box model under stationary state assumptions:

$$R = q \frac{C_{\text{in}} - C_{\text{out}}}{W}, \quad (4)$$

where R is the reaction rate for DOC or DO ($\text{nmol cm}^{-3} \text{h}^{-1}$), C_{in} and C_{out} are input and output concentrations, and W is the edge length of the box (5 cm here).

Statistical analyses, such as linear regression and one-way ANOVA, were conducted in Minitab (version 17). The alpha diversity of the microbial community, including Shannon index and equitability, Lefse LDA (Linear Discriminant Analysis) test for variability of microbiota, and PCA (Principal Component Analysis)/RDA (Redundancy Analysis) was calculated in the R environment. The statistical significance for all tests was assumed to be $\alpha = 0.05$. The plots of porewater and sediment profiles were constructed with SigmaPlot (version 12.5).

3. Results

3.1. Seawater and river water composition

Seawater salinity at high tides was approximately 34 in all seasons, while the seasonal variation of water temperature was much larger (Table 1). Seawater was always either saturated or oversaturated in DO. POC content fell within the range of 18.7 to 26.4 $\mu\text{mol L}^{-1}$. Concentrations of chlorophyll *a* were 3.24 to 4.86 $\mu\text{g L}^{-1}$, with the lowest values found in autumn. DOC concentrations ranged from 142 to 155 μM , with relative enrichment of labile materials compared to humic solutes (Table 1). DOC concentrations and α_{355} in the samples taken from the river were much higher than values from the bay water. However, $S_{275-295}$ in the river was much smaller than the seawater and the recalcitrant DOM was enriched in the Gu river (Table 1).

3.2. Porewater profiles at the seepage face

Salinity in the porewater collected at the seepage face ranged from 29.6 to 34.1 throughout the year (Table 2). The saltier porewater was found in the higher intertidal of the seepage face due to accumulation of recirculated seawater (Fig. 1B). In the medium and lower intertidal, porewater salinity decreased, especially in the deeper layer that was sampled, indicating the presence of terrestrial groundwater. The hydraulic head ranged from 2.7 to 10.9 cm, producing a discharge rate of 4.2 to 28.3 cm h^{-1} (Table 2). The porewater at the surface layer (0–2 cm depth) presented DO levels ranging from 70% to 86% saturation (Fig. S1). The difference in porewater DO saturation between the surface and bottom (20 cm) reached 13.9% in summer, indicating a significant DO consumption. In contrast, the lower value was obtained in winter.

DOC concentration in the sampled profiles ranged from 317 to 395 μM in spring (Fig. 2). Both DOC consumption (removal) and production (addition) were obtained during this season (Fig. 3A). The deep region (15–20 cm depth) acted as a DOC production zone, while the surface was active in DOC removal. A similar vertical distribution of DOC reaction rates was found in summer and autumn (Fig. 3B &

3C); nevertheless, DOC production shifted to the seepage face surface during winter (Fig. 3D). DOC reaction rates ranged from -54.9 (removal) to 68.9 (production) $\text{nmol C cm}^{-3} \text{h}^{-1}$ in spring (Fig. 3A). In summer, the porewater DOC concentration significantly decreased (Fig. 2 & Fig. 3F) while both production and removal rates increased (Fig. 3G). From autumn to winter, DOC reaction rates shrank. Among higher, medium and lower stations, both production and removal rates markedly varied in each season (Table S1). From spring to autumn, DOC removal in surface sediments was significantly weaker at the higher intertidal station compared to the other stations (Fig. 3H). Similar pattern was found in the production rate (bottom of the seepage face), whereas the large standard deviation led to insignificant differences among stations ($p = 0.18$).

The index of CDOM levels α_{355} varied between 1.4 and 2.0 in spring (Fig. 4). The increase in α_{355} was linked to DOC production (deep zone) and vice versa. In summer, α_{355} decreased in all profiles while the pattern remained (Fig. 4). For $S_{275-295}$, from spring to autumn, high values appeared in the bottom zone while low readings were found in the surface. In winter, both α_{355} and $S_{275-295}$ increased values were found in the sub-surface layer. Moreover, a significantly linear correlation between α_{355} and $S_{275-295}$ was observed ($R^2 = 0.53$, $p < 0.01$, $n = 108$; Fig. S1). Four types of FDOM solutes (two amino acid-like solutes and two humic-like materials) were identified with the PARAFAC analysis (detailed information in Table S2). During spring, tryptophan and tyrosine-like FDOM varied from 0.09 to 0.17 R.U. in the bottom of the studied sediment layer (20 cm depth). When depth decreased, the relative concentration of these two compounds increased, while a marked drop in the relative concentration in the surface (0–2 cm depth) was found. The relative concentrations of these labile compounds were tightly linked to α_{355} values in the porewater ($R^2 = 0.64$, $p < 0.01$, $n = 108$; Fig. S1). For humic-like materials (terrestrial and bacterial degradation), low concentrations were observed in the deeper sediment layer (< 0.18 R.U.). Towards the seepage face surface, a gradual accumulation of both humic materials in porewater was found (Fig. 4), peaking at the lower intertidal station. Similar vertical distributions of FDOM components in the porewater was found in the remaining sampling events.

3.3. Sediment physico-chemical parameters

In spring, SOC concentration varied between 77 and 116 $\mu\text{mol g}^{-1}$ (Fig. 5A) and the mean SOC concentration was 95 $\mu\text{mol g}^{-1}$, significantly higher than that of summer and autumn. Vertically, the higher levels of SOC were observed in the bottom at the three sampling stations within the seepage face from spring to autumn, while SOC enrichment shifted to the surface layer of the sediment in winter (Fig. S2). Similar to SOC, EOC concentration was also higher in the bottom and decreased towards the sediment surface (Fig. 5B). The mean EOC content ranged from 6.7 to 8.7 $\mu\text{mol g}^{-1}$ among four seasons, $< 10\%$ of the SOC inventory (Fig. 5E). The highest EOC concentration was also observed during spring, while the sediments in winter were relatively scarce in EOC (Fig. 5E). Chlorophyll *a* content ranged from 2.6 to 4.3 $\mu\text{g g}^{-1}$ in the sediment during spring (Fig. 5C). Apart from summer, the difference in mean sediment chlorophyll *a* concentration between the remaining seasons was statistically insignificant (Fig. 5F). Similar to SOC distribution in the sediment profile, both vertical EOC and chlorophyll *a* content increased with sediment depth from spring to autumn. In addition, these two organic pools were significantly correlated with SOC (EOC: SOC $R^2 = 0.31$, $p = 0.01$, $n = 60$; Chlorophyll *a*:SOC $R^2 = 0.59$, $p < 0.01$, $n = 60$, Fig. S1), indicating the importance of a pelagic source for the local SOC pool through seawater infiltration. In terms of the variation between different zones in the seepage face, minor differences in SOC, EOC and chlorophyll *a* were obtained. The value of α_{355} in the extraction solutions was also variable among the four seasons (Fig. S3). α_{355} increase was observed in the bottom (17–20 cm depth) in the seepage face, concomitantly with a reduction in the surface layer (spring, summer and autumn). Similar patterns were found in the

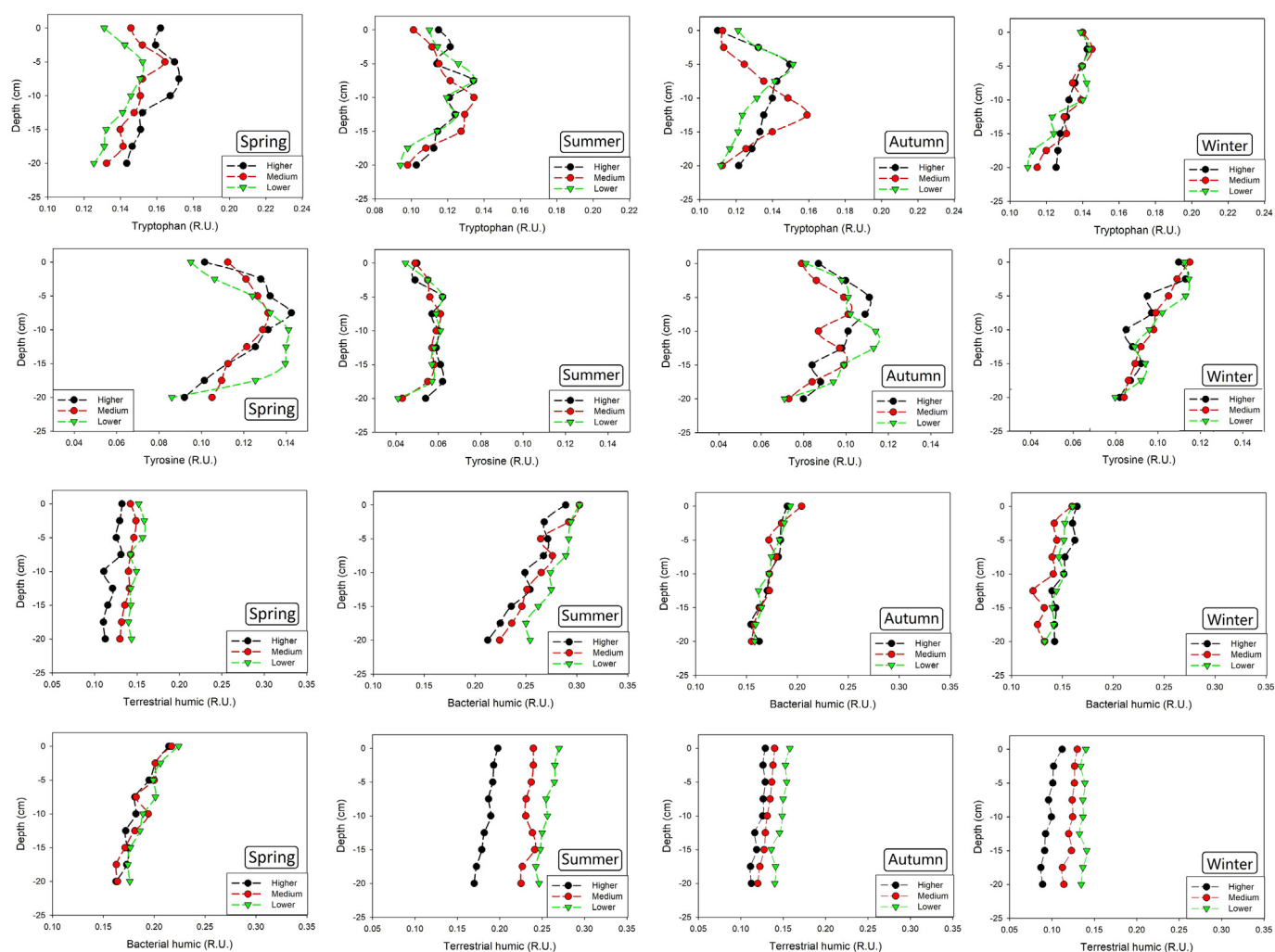


Fig. 3. DOC reaction rate ($\text{nmol C cm}^{-3} \text{ h}^{-1}$) in the sediment profile from spring (A) to winter (D). Positive rates indicate DOC addition while the negative rates indicate DOC removal. Mean reaction rates and deviation in three stations from spring to summer, highlighting the shift from DOC production to DOC removal along the sediment profile (E). Comparison of mean DOC reaction rates (F) between surface (0–2 cm, two layers) and bottom (15–17 cm, two layers) sediment and mean DOC concentrations and α_{355} and in porewater among four seasons (G). Comparison of mean DOC reaction rates among stations (H). Among four seasons, different characters, such as A and B, are added on top of bars. The difference in characters denotes a statistical significance ($p < 0.05$) between two groups.

distribution of $S_{275-295}$ and the two amino acid-like FDOM, while the difference of the two extracted humic-like FDOM materials between the surface and bottom sediments was minor (Fig. S3).

3.4. Benthic microbiota

Sediment microbial activity, quantified by the FDA hydrolysis potential, ranged from 22.4 to $31.5 \mu\text{g g}^{-1} \text{ h}^{-1}$ in spring (Fig. 5D). The highest microbial activity was found in the deeper end (17–20 cm depth) of the lower intertidal station. During summer, microbial activity significantly increased compared to the remaining seasons (Fig. 5F), peaking at $40.3 \mu\text{g g}^{-1} \text{ h}^{-1}$. OTUs of the sediment microbes ranged from 1145 to 1411 in spring (Table 3). During summer, OTUs markedly increased, reaching 4524 in the sediment surface. Coupled with an increase in OTUs, the Equitability and Shannon index increased (Table 3), suggesting benthic microbial diversity increase in metabolic reactions. The smallest OTU quantity was found in winter.

At the phylum-level, the most abundant species was *Proteobacteria*, accounting for 54% to 67% in the microbiota in spring (Fig. 6A). *Actinobacteria*, *Bacteroidetes*, and *Firmicutes* were also abundant in the sediment in spring. In other seasons, *Proteobacteria* was also the dominant species; nevertheless, the relative abundance decreased to

approximately 48% (summer). The opportunity species markedly varied among seasons, outlined by the Lefse LDA results (Fig. 7A). Compared with spring, the composition of *Acidobacteria*, *Actinobacteria* and *Thaumarchaeota* significantly increased in another 3 seasons. Accordingly, on the Bray Curtis tree and PCA analysis, sediment microbiota collected from different seasons were clearly separated at the phylum-level (Fig. 6A and Fig. 7B). The significantly seasonal difference was also observed at the class, order and family level for the determined sediment microbiota (Fig. S4).

At the genus-level, the *Pseudoalteromonas* was the dominant species (9.6% to 20.2% for the top-30 genus) in surface sediments in spring (Fig. 6B), while its portion slightly decreased in the deep zone. In comparison, *Marinobacter*, *Colwellia* and *Sphingobium* were enriched in the deep zone compared to the surface layer. RDA analysis revealed a tight linkage between sediment microbiota (OTU) and porewater DOC concentration (Fig. 7C). During summer, the dominant species shifted to *Nitrosopumilus* at the genus-level (4.5% to 16.5%) in sediments. *Thiopropfundum* was also an important species, accounting for 5.5% to 6.3% in all sediment microbes. The variation in the microbial community led to a clear separation on the cluster analysis. Furthermore, the linkage between sediment microbiota and humic materials was found during summer (Fig. 7C), indicating an active DOM degradation induced by heterotrophic microbes. During autumn, *Nitrosopumilus* was still the

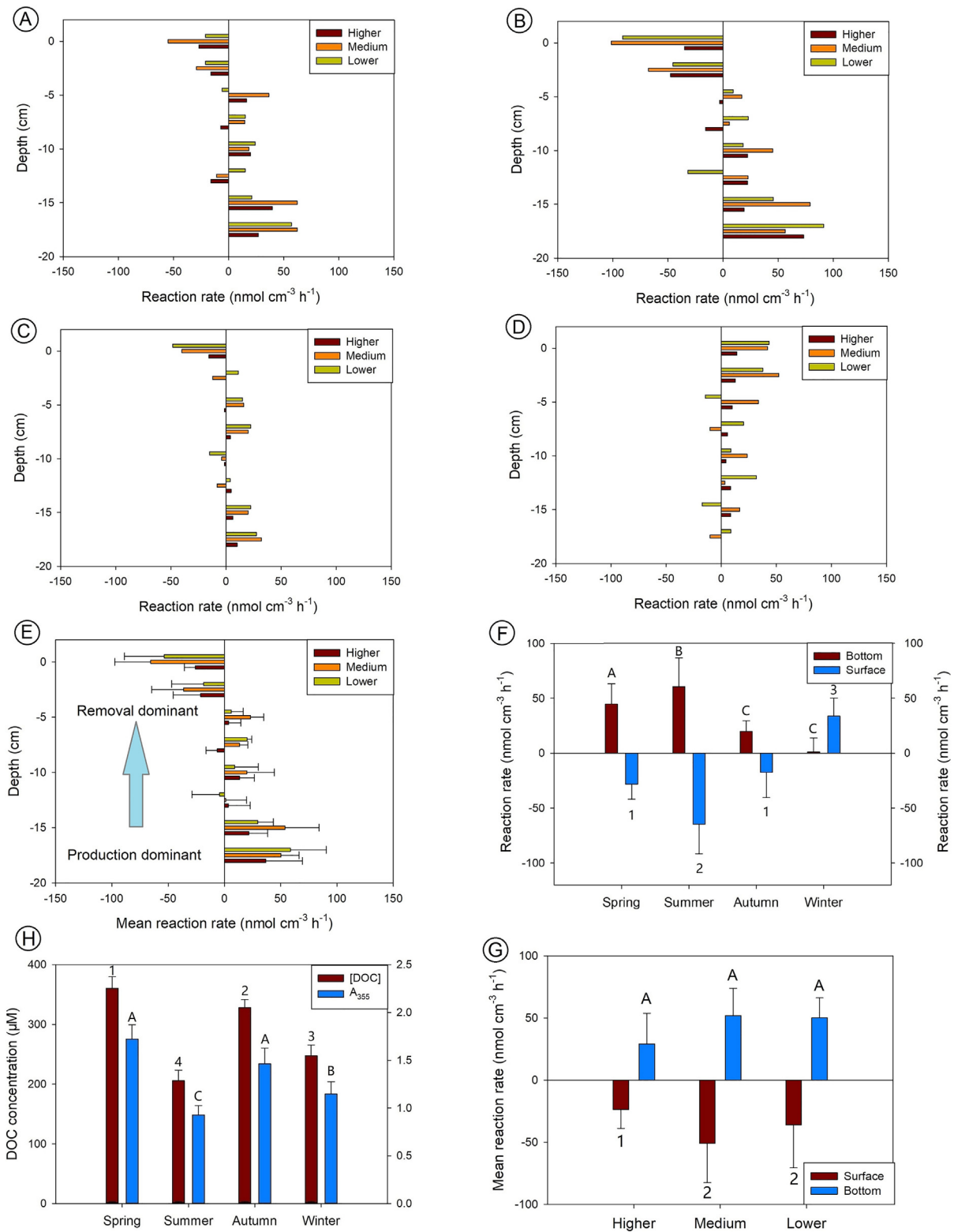


Fig. 4. Tryptophan like solute, Tyrosine like solute, Bacterial degradation produced humic material and Terrestrial humic in the porewater profile from three zones (higher, medium and lower) in the seepage face among four seasons.

dominant species at the genus-level, while the relative abundance of *Gp10*, *Ilumatobacter* and *Gp22* markedly increased, ranging from 0.96% to 4.81% (Fig. 6B). In winter, the relative abundance of all species at the genus-level was <10%. *Nitrosopumilus*, *Thiopropfundum*, *Gp10*, and *Ilumatobacter* were main components in the sediment microbial community.

4. Discussion

4.1. Active carbon turnover in the STE

STEs are the mixing zone between terrestrial groundwater and seawater and can be subject to significant advective transport (Rocha et al.,

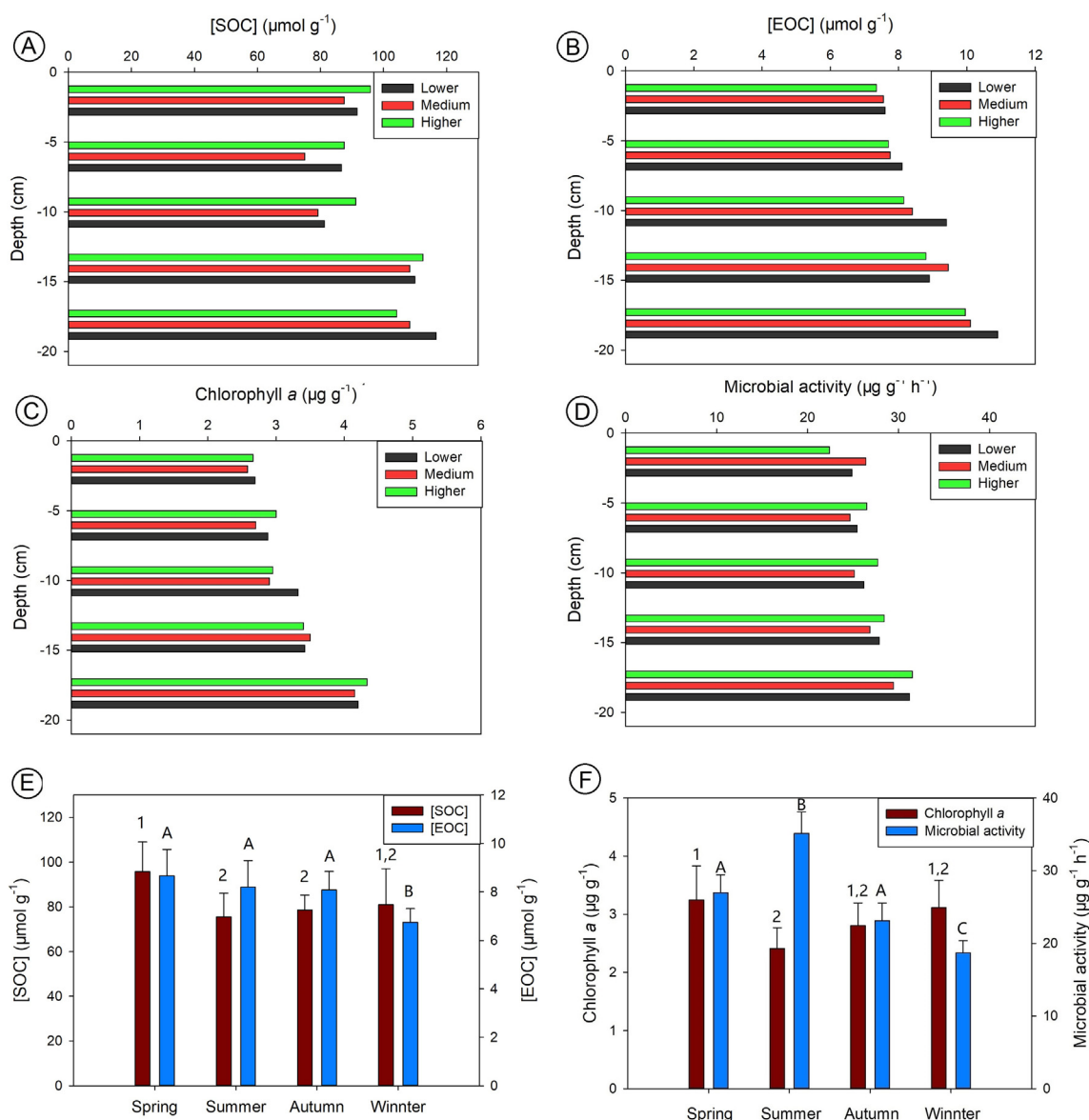


Fig. 5. SOC content (A), EOC content (B), Chlorophyll *a* content (C) and microbial activity (D) in sediment profiles during spring; (E) Comparisons of mean SOC and EOC among four seasons; (F) comparisons of sediment Chlorophyll *a* and microbial activity among four seasons. Different characters on top of bars, such as A and B, suggest a statistical significance ($p < 0.05$) between two groups.

Table 3

Microbial OTU number, Shannon index and related Equitability in surface (2 cm depth) and bottom (17 cm depth) sediments in the seepage face among four seasons.

Samples	Surface (2–5 cm)			Bottom (17–20 cm)		
	OTUs	Shannon	Equitability	OTUs	Shannon	Equitability
Spring-Higher	1411	8.52	0.815	1312	7.99	0.772
Spring-Medium	1145	7.43	0.731	1411	8.19	0.783
Spring-Lower	1288	7.33	0.709	1393	8.47	0.811
Summer-Higher	4524	9.42	0.776	3469	9.60	0.817
Summer-Medium	3974	9.23	0.772	4084	9.11	0.759
Summer-Lower	4354	9.22	0.762	2887	8.89	0.774
Autumn-Higher	2895	9.42	0.819	2604	8.98	0.791
Autumn-Medium	2938	9.36	0.812	2861	9.40	0.819
Autumn-Lower	2454	8.29	0.736	2417	8.90	0.792
Winter-Higher	934	8.03	0.814	6060	9.48	0.754
Winter-Medium	1262	8.50	0.825	4956	9.12	0.743
Winter-Lower	4279	9.33	0.774	4722	9.32	0.763

2009). In the present study, the discharge rate measured by the buried CTD-Diver in the seepage face ranged from 4.2 to 28.3 cm h^{-1} (Table 1). This record is comparable to peak discharge rates measured in the Ria Formosa Lagoon, Portugal ($>15 \text{ cm h}^{-1}$; Ibáñez and Rocha, 2016). It is also in line with the record of modeling results in a homogeneous beach (5.2 cm h^{-1} ; Evans and Wilson, 2016) and similar to the discharge rate measured by acoustic seepage meters ($<12.5 \text{ cm h}^{-1}$) and the dye dilution method ($<6.3 \text{ cm h}^{-1}$) in Waquoit Bay and Shelter Island, USA (Sholkovitz et al., 2003). Integrating the discharge rate measured along the seepage face, these ranged from 9.2 (winter) to 16.1 (summer) $\text{m}^2 \text{ d}^{-1}$, which were similar to the recirculated seawater discharge rate estimated by De Sieyes et al. (2008) in Stinson Beach, U.S. (22.9 to $31.7 \text{ m}^2 \text{ d}^{-1}$). The strong advection in place continuously transports solutes and benefits benthic reactions in SOC-limited sediments (Huetzel et al., 2014). As a response, the STE acted as an active reaction node for DOC transformation. DOC production rates varied from 2.3 to 91 $\text{nmol cm}^{-3} \text{ h}^{-1}$. The results are in line with those determined under controlled conditions (8.3 to 74.2 $\text{nmol cm}^{-3} \text{ h}^{-1}$) by Ibáñez

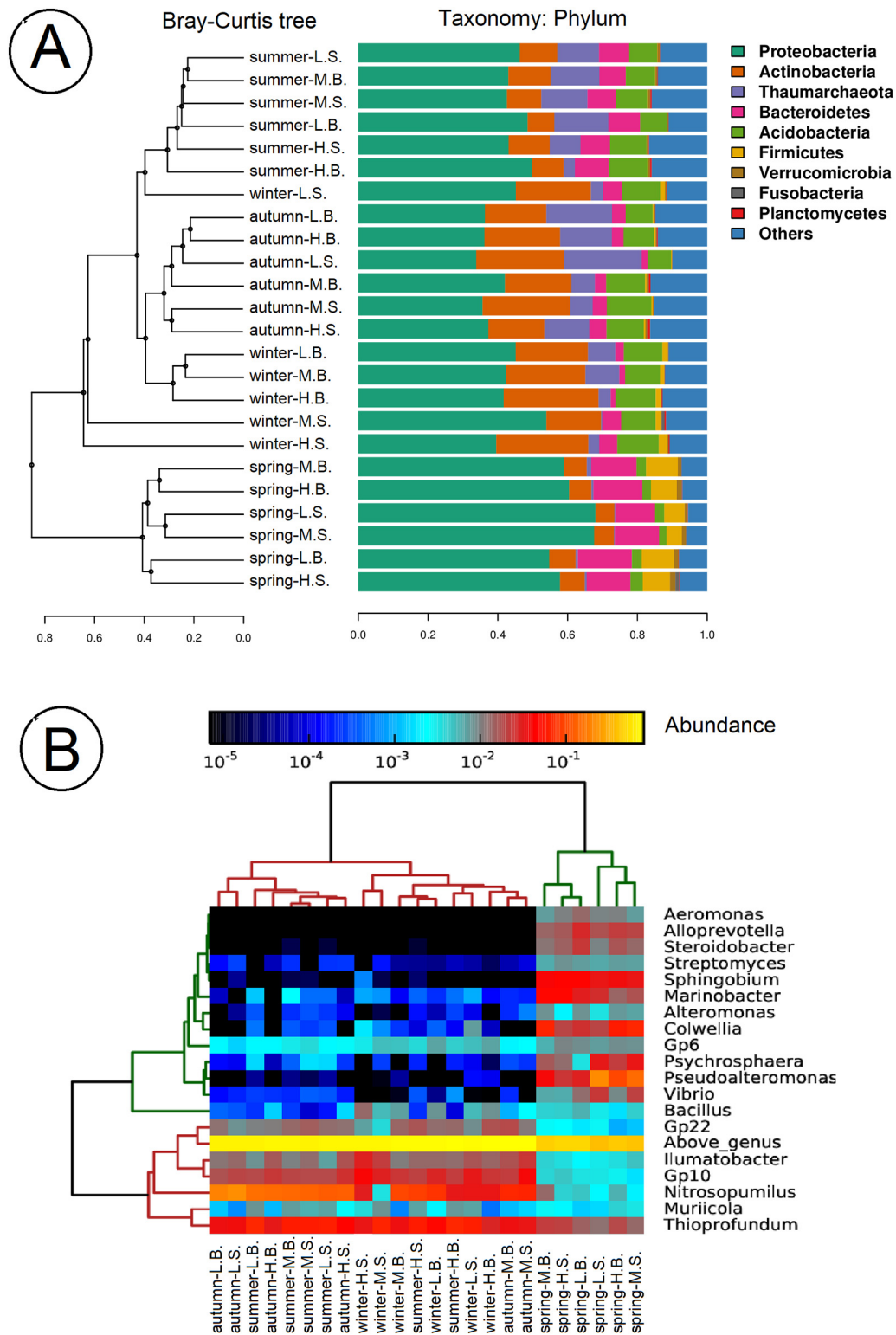


Fig. 6. Microbial community structure (relative abundance) on the phylum level among four seasons (A). It also highlights the seasonal variation in the community structure in the Bray-Curtis tree. In the figure, L indicates the lower intertidal site, M indicates the medium intertidal site, H indicates the higher intertidal site, S indicates the surface (2 cm) and B indicates the bottom (17 cm); (B) relative abundance of benthic microbes (genus level) among four seasons. It also shows the cluster results for the tested sediments.

and Rocha (2014) in Ria Formosa sediments. These rates are also comparable to the DOC production rates determined experimentally with sandy sediments from Dublin Bay, Ireland (1.5 to 6.2 $\text{nmol cm}^{-3} \text{h}^{-1}$; Jiang et al. submitted). Simultaneously, the surface sediment acted as a sink for DOC. DOC consumption was also observed in surface sediments of the Ria Formosa Lagoon (Ibáñez and Rocha, 2014). The DOC

removal rates found here ($<102 \text{ nmol cm}^{-3} \text{h}^{-1}$) are similar to DOC consumption rate ($113 \text{ nmol cm}^{-3} \text{h}^{-1}$) obtained with sediments from Ria Formosa with porewater amended with glucose (Jiang et al., 2018). These DOC production and consumption rates show that the STE in Sanggou Bay has the capacity to significantly modulate SGD-derived DOC fluxes from the beach aquifer to coastal waters.

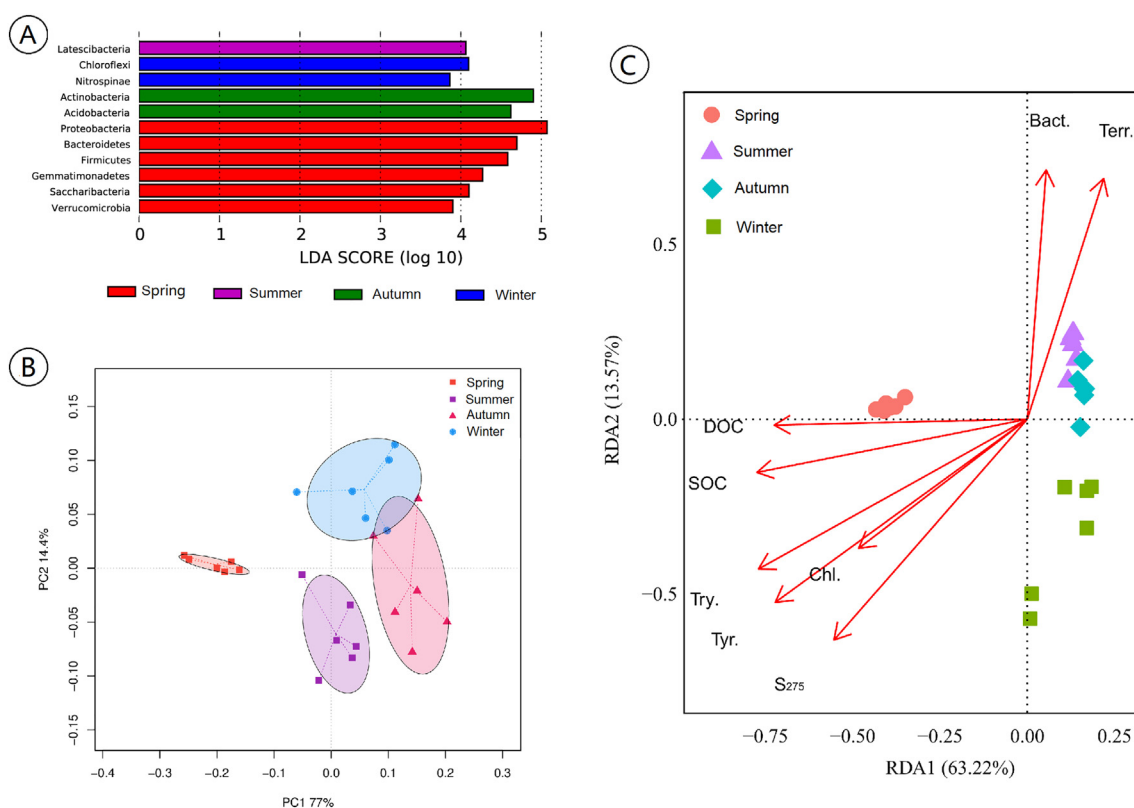


Fig. 7. Seasonal comparison of sediment microbiota using Lefse (Lda) test at the phylum level (A); (B) is PCA result for sediment microbial variability ($n = 24$) at the phylum level. (C) is RDA result for identification of the linkage between carbon factors and sediment microbiota (OTUs). To reduce the collinearity, a fraction of carbon factors was removed in the RDA analysis. In the figure, Chl. is chlorophyll *a*, Try. is tryptophan, Tyr. is Tyrosine, Terr. is terrestrial humic, Bact. is bacterial humic.

4.2. DOC production in the seepage face

From spring to autumn, DOC production was observed in the 15 to 20 cm depth layer of the studied seepage face. Increases in porewater DOC levels are usually linked to (1) desorption from sediment particles, driven by temperature and/or salinity variation, and (2) decomposition of the SOC, especially EOC, and subsequent release of dissolved fractions. Diel porewater temperature variations due to sunlight exposure are not expected in depth since all samplings occurred in evening. Furthermore, the salinity of the seeped water is generally lower than the surface seawater. Salinity decreases usually promotes the adsorption of DOC to sediment particles, potentially leading to a decline in porewater DOC concentration (Setia et al., 2013). Consequently, the contribution of desorption to the DOC increases observed in the seepage face is deemed negligible. Alternatively, SOC decomposition or degradation seems to be the main source of porewater DOC. The progressive accumulation of humic-like FDOM along the flow path, verified during all the surveys in the three stations, further supports the idea of active heterotrophic processing of organic matter in the studied sediment column.

The most significant feature is the enrichment of SOC in the bottom sediment. This fraction might result from the infiltration of suspended particles during tidally-driven porewater-seawater exchange together with sediment reworking by waves, as suggested by the in-depth maximum of chlorophyll *a* observed. Seawater can intrude into the seepage face at high tides if the pressure balance between the coastal aquifer and surface seawater permits, or directly into the undersaturated, upper intertidal. Particulate organic matter is thus retained within the sediment, leading to the periodical supply of new SOC, including labile fractions, such as phytoplankton debris and feces from clams and abalone culture. SOC is then decomposed and degraded producing DOC via

heterotrophic metabolism as suggested by the significant correlation between SOC and microbial activity (Fig. S1).

During each season (excluding winter), the difference in SOC and EOC concentration in the bottom sediments among three stations was minor (e.g. Fig. 5A & B). Concurrently, microbial activity and community structure, e.g. dominant species, were also similar in the bottom among the three intertidal stations (Fig. 6A). Theoretically, this similarity could lead to a minor variation in the DOC production rate among stations. In contrast, DOC production rates obtained in the deeper studied sediment (20 cm) in the medium and the lower intertidal were frequently higher than values found in the higher intertidal station, especially autumn (c.f. Fig. 3A to C). The mean production rate (spring to autumn) at the higher intertidal station was also smaller than the remaining seasons (Fig. 3F). This apparent contradiction reveals the significance of advection rate on the coupling between SOC degradation and DOC production (Ehrenhauss and Huettel, 2004). In particular, in the medium and lower intertidal, advection rate was significantly higher compared to the upper beach levels, because of the large hydraulic head (Table 1). Increasing advection delivers higher quantities of reactants for microbially mediated reactions (e.g. DO from surface seawater) while removing metabolic products benefiting microbial reactions on the particle surface (Boudreau et al., 2001; Ibáñez and Rocha, 2017).

Apart from the spatial difference along the intertidal, seasonal variations in the DOC production rate were also observed (Fig. 3A to D), probably as the result of changes in porewater temperature and advection rate (Thamdrup et al., 1998; Brin et al., 2015; Ibáñez and Rocha, 2016). More importantly, changes in the benthic microbial community also seemed to influence DOC processing. Carbon utilization preference varies markedly among different species. For instance, at the phylum-level, during spring, *Proteobacteria* ranged from 54.5% to 67.2% while *Thaumarchaeota* was minor (Fig. 6A). In contrast, during autumn,

Proteobacteria decreased to 38.1%, while the abundance of *Thaumarchaeota* markedly increased, peaking at 16.9%. Generally, the majority of *Proteobacteria* are heterotrophic, requiring an external energy supply (Kersters et al., 2006), while *Thaumarchaeota* oxidizes NH_4^+ to sustain metabolism (Kozłowski et al., 2016). The enrichment of *Proteobacteria* benefits SOC decomposition and a fraction of DOC, including labile fractions, might be released into the porewater. At the genus-level, *Pseudoalteromonas*, the dominant species in spring, is characterized as highly active in degradation of large molecular organic fractions, such as fucoidan (Bakunina et al., 2002) and chitin (Techkarnjanaruk and Goodman, 1999), suggesting that *Pseudoalteromonas* might be suitable for the degradation of refractory SOC. In contrast, *Nitrosopumilus* might be active in the use of small molecular compounds, e.g. glucose, mannose and inositol (Könneke et al., 2012), and organic pollutants, e.g. pentabromodiphenyl ether (Yan et al., 2017). These characteristics suggest that benthic microbes in spring are more efficient in SOC decomposition-DOC production compared with the microbes in autumn. The RDA analysis further reinforced the tight linkage between DOC production and sediment microbiota during spring (Fig. 7C). The microbial activity also influences DOC production. During summer, microbiota was similar to that observed in autumn at both phylum-level and genus-level (Fig. 6A). The low abundance of *Proteobacteria* suggests a slow DOC production rate. However, the microbial activity in summer was the highest measured (Fig. 5F). Such high activity could drive a rapid transformation of SOC, leading to a significant DOC accumulation in porewater. Thus, the stimulated microbial activity might play more vital role in DOC production compared to the benthic microbial community structure.

A seasonal shift in the depth of the net DOC production zone was also observed. From spring to autumn, the DOC production occurred in 15–20 cm depth, while it moved to the surface in winter (Fig. 3). Considering the similar wave height and tidal amplitude during each sampling and the minor difference in the grain size among seasons, the shift likely results from the change in the pelagic input, especially plankton debris because of the tight relationship between SOC and chlorophyll *a*. In particular, the microbial and phytodegradation of phytoplankton debris (large pieces to small pieces) would be higher in the warmer bay waters (summer) and lower during the winter (Chen and Wangersky, 1996). A similar reaction pattern could be found in the feces from clam and abalone. The active microbial breakdown in the bay water likely produces smaller pieces of the detritus, which could easily seep into the deep layer of the seepage face during recharge (outlined in Fig. 1B). In contrast, mild degradation produces a large piece of particles, only depositing on the surface of the sediment. Besides degradation, phytoplankton species variation might also be an explanation. In Sanggou Bay, the dominant species is diatom, while dinoflagellates rapidly increase in spring and summer (Yuan et al., 2014). Compared to diatoms, the size/diameter of dinoflagellates is frequently much smaller (Hitchcock, 1982), suggesting the potential for transport deeper into the sediments.

4.3. DOC removal in the seepage face

In contrast with winter, a fraction of produced DOC was rapidly removed in the sediment surface from spring to autumn. The removal of DOC in surface sediments was also reported in the Lake Urmere, Switzerland (Davis, 1982) and the Ria Formosa Lagoon, Portugal (Ibáñez and Rocha, 2016). DOC removal in sandy sediments might result from adsorption, as aforementioned. However, compared to the bottom layer (15–20 cm depth), both SOC and EOC of the surface sediment were lower, suggesting that DOC sorption might be low. Alternatively, aerobic respiration could be an important pathway for DOC removal, particularly under the high DO levels measured in the studied sediment column in all the sampling events (Fig. 2A). As aforementioned, microbes at the phylum of *Proteobacteria*, is heterotrophic. At the genus-level, dominant species of *Pseudoalteromonas* and

Nitrosopumilus are also heterotrophic, especially microbes of *Nitrosopumilus* strongly rely on the supply of labile organic carbon in the culture medium (Elling et al., 2014). For the opportunity species, apart from *Thiopfundum* that is chemolithoautotrophic (Mori et al., 2011), *Colwellia* and *Gp10* are in significant requirement of exogenous organic matter (Huston et al., 2004; Liu et al., 2014). Apart from the accumulation of humic-like FDOM along the flow path in the entire sediment column studied that suggests active organic matter processing, labile FDOM was also being produced in the deeper sediment layers. Nevertheless, in the sediment surface, net DOC consumption occurs concomitantly with labile FDOM consumption. This suggests a change in the organic matter source used for heterotrophic processes. Along the flow path, progressively lower SOC, EOC and chlorophyll *a*, suggesting a shortage of the labile proportion in the SOC, and increased DOC and labile FDOM in the porewater promote a shift towards higher utilization of DOC for heterotrophic processes towards the sediment surface. In laboratory culture, *Nitrosopumilus* directly utilize DOC from the culture medium (Könneke et al., 2012). *Gp22* (*Actinobacteria*) is in favor of small molecular organic acids in soils (Li et al., 2014). These key species could be versatile in benthic environments, shifting between SOC and DOC utilization on the basis of availability (concentration and labile fractions).

Similar to DOC production, a seasonal variation in the DOC removal rate in the sediment surface occurred. During summer, the DOC concentration and CDOM levels were the lowest compared to porewater obtained in both spring and autumn. The labile fractions, such as amino-acid like FDOM, were also minor in summer (Fig. 2), concomitantly with the highest DOC removal rates found (Fig. 3E). Such discrepancy can be explained by temperature-dependent microbial activities. More importantly, given the positive correlation between benthic microbes and humic materials as revealed by the RDA result (Fig. 7C), the sediment microbiota may also play a key role in the DOC removal during summer. In particular, soil/sediment microbes have a wide selection of carbon sources, ranging from small molecular compounds, e.g. fatty acids (Slater et al., 2005), organic acids (Li et al., 2014), to polymers, e.g. lignin (Yu et al., 2018). The low supply of labile compounds might trigger the enhancement in degradations of large molecular DOM via accelerating the synthesis of related enzymes (e.g. glucose–lactose diauxic experiments; Inada et al., 1996). Furthermore, a number of sediment microbes might be associated with a series of metabolism reactions. The products, e.g. Fe^{2+} and Mn^{2+} from reduction, could be important reactants for carbon oxidation (Canfield et al., 1993). During summer, the highest OTU number, Shannon index and Equability were found (Table 3), indicating a higher diversity of sediment microbes participated in the benthic metabolism. Adding these together, the low porewater DOC concentration produced the highest reaction rate.

During winter, DOC production dominated in the surface sediment, concomitantly with the higher SOC levels available along the sediment vertical profile. It suggests that the degradation of labile SOC, e.g. phytoplankton detritus, is the preferable source of carbon and electrons for benthic microbes. Furthermore, the microbial activity in the surface sediment was lower than the value in the deep layer (production zone). It reinforced that SOC plays an important role in benthic reactions due to the direct contact with sediment microbes (Jiang et al., 2018), while DOC may not be the primary target in the microbe-mediated biogeochemical reactions if high-level SOC, especially EOC and labile DOM, are available.

4.4. Estimates of SGD-borne DOC fluxes to the coastal zone

SGD contributes a significant quantity of DOC in many coastal systems worldwide (e.g. Okatee River estuary, U.S.A., Porubsky et al., 2014; Korogoro Creek, Australia; Sadat-Noori et al., 2016; Maowei Sea, China; Chen et al., 2018). Here, DOC concentration in the outflowing porewater increased compared to surface seawater due to strong DOC production within the seepage face. DOC loading via SGD ranged from

0.39 to 1.85 $\text{g m}^{-2} \text{d}^{-1}$ in the different intertidal stations sampled in the Sanggou Bay seepage face (Fig. 8A). These rates fall in a similar range to results obtained in the sub-tropical coastal line of the Maowei Sea (3 to 3.7 $\text{g m}^{-2} \text{d}^{-1}$; Chen et al., 2018) and the Okatee Estuary, USA (2.0 $\text{g m}^{-2} \text{d}^{-1}$; Moore et al., 2006), where intensive primary production was observed. In addition, compared to the turnover rate obtained from temperate zones, such as the Yarra River estuary, Australia and the Hampyeong Bay, Korea, the DOC production in the Sanggou Bay is markedly higher (Fig. 8B). These comparisons reinforced the rapid carbon turnover in the seepage face at Sanggou Bay, stimulated with the periodical tidal supply of abundant phytoplankton and detritus to the seepage face.

Integrating the sampled beach profile, the magnitude of SGD borne DOC flux to Sanggou Bay ranged from 28.5 to 43.3 $\text{g C m}^{-1} \text{d}^{-1}$, peaking in summer due to the high discharge rate. Compared to the DOC loading via the Gu River (Fig. 8C & D), SGD was a minor contributor to the bay DOC inventory (varying between 8.6% in summer to 12.5% and winter). In addition, the river was a net source of POC, while the STE acted as a net reactive sink for POC. Because of the strong degradation, a significant accumulation of labile fractions of DOM was observed in porewater and the seepage outflow. This is in contrast to the findings suggesting SGD is mainly a source of recalcitrant DOM from karst systems into the sea (e.g. Kinvara Bay, Ireland; Kelly, 2018), suggesting an important transformative role played by non-karstic STEs in labile DOM production and export. Therefore, the environmental function of the STE in Sanggou Bay is a 'filter' for POC and a source of labile DOC. In the bay, POC would have accumulated in the benthos, potentially increasing local oxygen consumption. The removal in subterranean estuary may

decrease the possibility of carbon-dependent hypoxia occurrence. The produced DOC, especially the labile fraction, is likely to be rapidly utilized by primary producers and heterotrophic prokaryotes along the coastal belts, sustaining the ecological and environmental functions in the bay.

5. Conclusions

The seepage face in Sanggou Bay is an active benthic reactor for carbon cycling, hosting detritus degradation-based DOC production and aerobic respiration/biological assimilation-based DOC removal. The porewater flow rate was the key driver for the rates of these reactions, explaining marked variations observed between stations and seasons. Changes in the microbiota also impact benthic microbial reactivity. An increase in relative abundance of exclusive heterotrophic species (e.g. *Pseudoalteromonas* and *Nitrosopumilus*) accelerates carbon transformation rates, especially when the sediment microbial activity was stimulated by porewater high temperature. Spatial separation between net DOC production (15–20 cm depth) and net DOC removal (0–5 cm surface) was observed year around except in winter, likely resulting from variations in the quantity and quality of the SOC pool. During winter, the location of the net DOC production zone moved to the surface, in parallel with a shift in the zone of higher SOC content. Among four seasons, the STE in Sanggou Bay acted as a source of DOC, via active processing of infiltrated pelagic POC. This pelagic POC consumption reduces the likelihood of benthic hypoxia driven by carbon accumulation in the bay bottom zone.

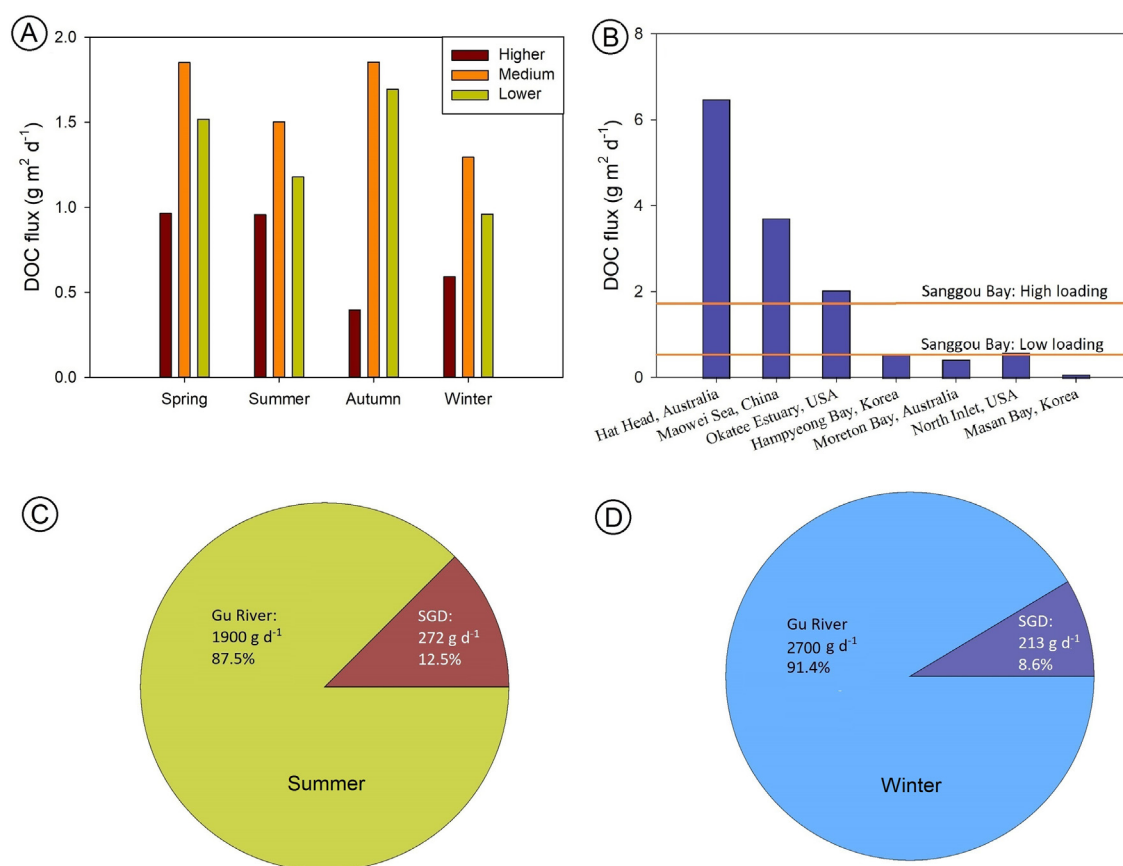


Fig. 8. (A) the magnitude of DOC flux from the seepage face to the Bay; (B) a global comparison of SGD borne DOC loading among the present study and other coastal systems: Hat Head (Sadat-Noori et al., 2016); Maowei Sea (Chen et al., 2018); Okatee Estuary (Moore et al., 2006); Hampyeong Bay (Kim et al., 2012); Moreton Bay (Maher et al., 2013); North Inlet (Goñi and Gardner, 2003) and Masan Bay (Oh et al., 2017); (C) and (D) show the comparison of SGD derived DOC loading (7.5 km STE length) to the Gu River derived DOC loading in the summer and winter, respectively. The magnitude of DOC flux from the subterranean estuary was estimated as the intergration of DOC loading from the seepage face and a multiplication constant (2; Li et al., 2008).

CRedit authorship contribution statement

Shan Jiang: Conceptualization, Investigation, Methodology, Writing - original draft, Project administration, Funding acquisition. **Yixue Zhang:** Investigation. **Jie Jin:** Investigation. **Ying Wu:** Methodology, Resources, Writing - original draft. **Yongjun Wei:** Formal analysis, Writing - original draft. **Xiaolu Wang:** Investigation. **Carlos Rocha:** Methodology, Writing - original draft. **Juan Severino Pino Ibáñez:** Methodology, Writing - original draft. **Jing Zhang:** Conceptualization, Resources, Writing - original draft, Funding acquisition.

Declaration of competing interest

The authors declare that they have no conflict of interest.

Acknowledgment

This work was supported by the National Natural Science Foundation of China (41706081) and Scientific Research Foundation of SKLEC (2017RCDW04). Technical support and suggestions during the laboratory analyses by Ying Cui, Guosen Zhang and Miao Zhang in East China Normal University and Mark Kavanagh at Trinity College Dublin are gratefully acknowledged. We also appreciate DeepBiome Co., Ltd. for bioinformatic assistance.

Appendix A. Supplementary data

Supplementary data to this article can be found online at <https://doi.org/10.1016/j.scitotenv.2020.138220>.

References

- Bakunina, I.Y., Nedashkovskaya, O.I., Alekseeva, S.A., Ivanova, E.P., Romanenko, L.A., Gorshkova, N.M., Isakov, V.V., Zvyagintseva, T.N., Mikhailov, V.V., 2002. Degradation of fucoidan by the marine *Proteobacterium Pseudoalteromonas citrea*. *Microbiol* 71, 41–47.
- Bauer, J.E., Cai, W.J., Raymond, P.A., Bianchi, T.S., Hopkinson, C.S., Regnier, P.A.G., 2013. The changing carbon cycle of the coastal ocean. *Nature* 504, 61.
- Bianchi, T.S., 2011. The role of terrestrially derived organic carbon in the coastal ocean: a changing paradigm and the priming effect. *PNAS* 108, 19473–19481.
- Boudreau, B.P., Huettel, M., Forster, S., Jahnke, R.A., McLachlan, A., Middelburg, J.J., Nielsen, P., Sansone, F., Taghon, G., Van Raaphorst, W., Webster, I., Weslawski, J.M., Wiberg, P., Sundby, B., 2001. Permeable marine sediments: overturning an old paradigm. *EOS Transactions* 82, 133–136.
- Brin, L.D., Giblin, A.E., Rich, J.J., 2015. Effects of experimental warming and carbon addition on nitrate reduction and respiration in coastal sediments. *Biogeochemistry* 125, 81–95.
- Canfield, D.E., Thamdrup, B., Hansen, J.W., 1993. The anaerobic degradation of organic matter in Danish coastal sediments: iron reduction, manganese reduction, and sulfate reduction. *Geochim. Cosmochim. Acta* 57, 3867–3883.
- Castle, S.C., Morrison, C.D., Barger, N.N., 2011. Extraction of chlorophyll a from biological soil crusts: a comparison of solvents for spectrophotometric determination. *Soil Biol. Biochem.* 43, 853–856.
- Cebrian, J., 2002. Variability and control of carbon consumption, export, and accumulation in marine communities. *Limnol. Oceanogr.* 47, 11–22.
- Charbonnier, C., Anschutz, P., Poirier, D., Bujan, S., Lacroix, P., 2013. Aerobic respiration in a high-energy sandy beach. *Mar. Chem.* 155, 10–21.
- Chen, W., Wangersky, P.J., 1996. Rates of microbial degradation of dissolved organic carbon from phytoplankton cultures. *J. Plan. Res.* 18, 1521–1533.
- Chen, X., Zhang, F., Lao, Y., Wang, X., Du, J., Santos, I.R., 2018. Submarine groundwater discharge-derived carbon fluxes in mangroves: an important component of blue carbon budgets? *J. Geophys. Res.-Oceans* 123, 6962–6979.
- Chipman, L., Podgorski, D., Green, S., Kostka, J., Cooper, W., Huettel, M., 2010. Decomposition of plankton-derived dissolved organic matter in permeable coastal sediments. *Limnol. Oceanogr.* 55, 857–871.
- Couturier, M., Nozais, C., Chaillou, G., 2016. Microtidal subterranean estuaries as a source of fresh terrestrial dissolved organic matter to the coastal ocean. *Mar. Chem.* 186, 46–57.
- Davis, J.A., 1982. Adsorption of natural dissolved organic matter at the oxide/water interface. *Geochim. Cosmochim. Acta* 46, 2381–2393.
- De Sieyes, N.R., Yamahara, K.M., Layton, B.A., Joyce, E.H., Boehm, A.B., 2008. Submarine discharge of nutrient-enriched fresh groundwater at Stinson Beach, California is enhanced during neap tides. *Limnol. Oceanogr.* 53, 1434–1445.
- Edgar, R.C., 2013. UPARSE: highly accurate OTU sequences from microbial amplicon reads. *Nat. Methods* 10, 996.
- Edgar, R.C., 2016. SINTAX: a simple non-Bayesian taxonomy classifier for 16S and ITS sequences. *bioRxiv*, 074161 <https://doi.org/10.1101/074161>.
- Edgar, R.C., Flyvbjerg, H., 2015. Error filtering, pair assembly and error correction for next-generation sequencing reads. *Bioinformatics* 31, 3476–3482.
- Ehrenhauss, S., Huettel, M., 2004. Advective transport and decomposition of chain-forming planktonic diatoms in permeable sediments. *J. Sea Res.* 52 (3), 179–197.
- Elling, F.J., Könneke, M., Lipp, J.S., Becker, K.W., Gagen, E.J., Hinrichs, K.-U., 2014. Effects of growth phase on the membrane lipid composition of the thaumarchaeon *Nitrosopumilus maritimus* and their implications for archaeal lipid distributions in the marine environment. *Geochim. Cosmochim. Acta* 141, 579–597.
- Evans, T.B., Wilson, A.M., 2016. Groundwater transport and the freshwater–saltwater interface below sandy beaches. *J. Hydrol.* 538, 563–573.
- Fang, J., Zhang, J., Xiao, T., Huang, D., Liu, S., 2016. Integrated multi-trophic aquaculture (IMTA) in Sanggou Bay, China. *Aquac. Environ. Interact.* 8, 201–205.
- Goñi, M.A., Gardner, I.R., 2003. Seasonal dynamics in dissolved organic carbon concentrations in a coastal water-table aquifer at the forest-marsh interface. *Aquat. Geochem.* 9, 209–232.
- Hitchcock, G.L., 1982. A comparative study of the size-dependent organic composition of marine diatoms and dinoflagellates. *J. Plankton Res.* 4 (2), 363–377.
- Hou, J., Zhang, G., Sun, M., Ye, W., Song, D., 2016. Methane distribution, sources, and sinks in an aquaculture bay (Sanggou Bay, China). *Aquacult. Environ. Interact.* 8, 481–495.
- Huettel, M., Ziebis, W., Forster, S., Luther, G.W., 1998. Advective transport affecting metal and nutrient distributions and interfacial fluxes in permeable sediments. *Geochim. Cosmochim. Acta* 62, 613–631.
- Huettel, M., Berg, P., Kostka, J.E., 2014. Benthic exchange and biogeochemical cycling in permeable sediments. *Annu. Rev. Mar. Sci.* 6, 23–51.
- Huston, A.L., Methe, B., Deming, J.W., 2004. Purification, characterization, and sequencing of an extracellular cold-active aminopeptidase produced by marine psychrophile *Colwellia psychrerythrae* strain 34H. *Appl. Environ. Microb.* 70, 3321–3328.
- Ibáñez, J.S.P., Rocha, C., 2014. Effects of recirculation of seawater enriched in inorganic nitrogen on dissolved organic carbon processing in sandy seepage face sediments. *Mar. Chem.* 166, 48–58.
- Ibáñez, J.S.P., Rocha, C., 2016. Oxygen transport and reactivity within a sandy seepage face in a mesotidal lagoon (Ria Formosa, Southwestern Iberia). *Limnol. Oceanogr.* 61, 61–77.
- Ibáñez, J.S.P., Rocha, C., 2017. Kinetics of inorganic nitrogen turnover in a sandy seepage face on a subterranean estuary. *Appl. Geochem.* 87, 108–121.
- Ibáñez, J.S.P., Leote, C., Rocha, C., 2011. Porewater nitrate profiles in sandy sediments hosting submarine groundwater discharge described by an advection–dispersion–reaction model. *Biogeochemistry* 103, 159–180.
- Inada, T., Kimata, K., Aiba, H., 1996. Mechanism responsible for glucose–lactose diauxie in *Escherichia coli*: challenge to the cAMP model. *Genes Cells* 1, 293–301.
- Jiang, Z., Li, J., Qiao, X., Wang, G., Bian, D., Jiang, X., Liu, Y., Huang, D., Wang, W., Fang, J., 2015. The budget of dissolved inorganic carbon in the shellfish and seaweed integrated mariculture area of Sanggou Bay, Shandong, China. *Aquaculture* 446, 167–174.
- Jiang, S., Huang, J., Lu, H., Liu, J., Yan, C., 2016. Optimisation for assay of fluorescein diacetate hydrolytic activity as a sensitive tool to evaluate impacts of pollutants and nutrients on microbial activity in coastal sediments. *Mar. Pollut. Bull.* 110, 424–431.
- Jiang, S., Kavanagh, M., Rocha, C., 2017. Evaluation of the suitability of vacuainers for storage of nutrient and dissolved organic carbon analytes in water samples. *Biol. Environ.* 33–46.
- Jiang, S., Ibáñez, J.S.P., Rocha, C., 2018. Influence of labile dissolved organic matter on nitrate reduction in a seepage face. *Environ. Sci. Pollut. R.* 25, 10654–10667.
- Jiang, S., Kavanagh, M., Ibáñez, J.S.P., Rocha, C., Submitted. Nitrate production and removal in permeable coastal sediments: an investigation on the effect of salinity and nitrate supply condition using flow-through reactors. *Environ. Sci. Pollut. R.*
- Kelly, T., 2018. An Investigation of the Effects of Submarine Groundwater Discharge on the Coastal Carbon and Nutrient Cycles of a Karstic Aquifer. Trinity College Dublin, Kinvara Bay, Co Galway, Ireland.
- Kerstens, K., De Vos, P., Gillis, M., Swings, J., Vandamme, P., Stackebrandt, E., 2006. Introduction to the Proteobacteria. In: Dworkin, M., Falkow, S., Rosenberg, E., Schleifer, K.H., Stackebrandt, E. (Eds.), *The Prokaryotes*. Springer, New York, NY.
- Kim, T.H., Waska, H., Kwon, E., Suryaputra, I.G.N., Kim, G., 2012. Production, degradation, and flux of dissolved organic matter in the subterranean estuary of a large tidal flat. *Mar. Chem.* 142–144, 1–10.
- Könneke, M., Lipp, J.S., Hinrichs, K.U., 2012. Carbon isotope fractionation by the marine ammonia-oxidizing archaeon *Nitrosopumilus maritimus*. *Org. Geochem.* 48, 21–24.
- Kozłowski, J.A., Stieglmeier, M., Schleper, C., Klotz, M.G., Stein, L.Y., 2016. Pathways and key intermediates required for obligate aerobic ammonia-dependent chemolithotrophy in bacteria and Thaumarchaeota. *The ISME Journal* 10, 1836.
- Li, H., Boufadel, M.C., Weaver, J.W., 2008. Tide-induced seawater-groundwater circulation in shallow beach aquifers. *J. Hydrol.* 352, 211–224.
- Li, X., Rui, J., Mao, Y., Yannarell, A., Mackie, R., 2014. Dynamics of the bacterial community structure in the rhizosphere of a maize cultivar. *Soil Biol. Biochem.* 68, 392–401.
- Liu, P.W.G., Chang, T.C., Chen, C.H., Wang, M.Z., Hsu, H.W., 2014. Bioaugmentation efficiency investigation on soil organic matters and microbial community shift of diesel-contaminated soils. *Int. Biodeterior. Biodegradation* 95, 276–284.
- Ma, Q., Li, H., Wang, X., Wang, C., Wan, L., Wang, X., Jiang, X.J., 2015. Estimation of seawater-groundwater exchange rate: case study in a tidal flat with a large-scale seepage face (Laizhou Bay, China). *Hydrogeol. J.* 23, 265–275.
- Maher, D.T., Santos, I.R., Golsby-Smith, L., Gleeson, J., Eyre, B.D., 2013. Groundwater-derived dissolved inorganic and organic carbon exports from a mangrove tidal creek: the missing mangrove carbon sink? *Limnol. Oceanogr.* 58, 475–488.
- Marchant, H.K., Ahmerkamp, S., Lavik, G., Tegetmeyer, H.E., Graf, J., Klatt, J.M., Holtappels, M., Walpersdorf, E., Kuypers, M.M.M., 2017. Denitrifying community in coastal sedi-

- ments performs aerobic and anaerobic respiration simultaneously. The ISME Journal 11, 1799–1812.
- Moore, W.S., 1999. The subterranean estuary: a reaction zone of ground water and sea water. *Mar. Chem.* 65, 111–125.
- Moore, W.S., 2010. The effect of submarine groundwater discharge on the ocean. *Annu. Rev. Mar. Sci.* 2, 59–88.
- Moore, W.S., Blanton, J.O., Joye, S.B., 2006. Estimates of flushing times, submarine groundwater discharge, and nutrient fluxes to Okatee Estuary, South Carolina. *J. Geophys. Res.-Oceans* 111, C09006.
- Mori, K., Suzuki, K., Urabe, T., Sugihara, M., Tanaka, K., Hamada, M., Hanada, S., 2011. *Thiopseudomonas hispidum* sp. nov., an obligately chemolithoautotrophic sulfur-oxidizing gammaproteobacterium isolated from the hydrothermal field on Suiyo Seamount, and proposal of *Thioalkalispiraceae* fam. nov. in the order Chromatiales. *Int. J. Syst. Evol. Microb.* 61, 2412–2418.
- Oh, Y.H., Lee, Y.W., Park, S.R., Kim, T.H., 2017. Importance of dissolved organic carbon flux through submarine groundwater discharge to the coastal ocean: results from Masan Bay, the southern coast of Korea. *J. Marine Syst.* 173, 43–48.
- Porubsky, W., Weston, N., Moore, W., Ruppel, C., Joye, S., 2014. Dynamics of submarine groundwater discharge and associated fluxes of dissolved nutrients, carbon, and trace gases to the coastal zone (Okatee River estuary, South Carolina). *Geochim. Cosmochim. Acta* 131, 81–97.
- Probandt, D., Knittel, K., Tegetmeyer, H.E., Ahmerkamp, S., Holtappels, M., Amann, R., 2017. Permeability shapes bacterial communities in sublittoral surface sediments. *Environ. Microbiol.* 19, 1584–1599.
- Rocha, C., 1998. Rhythmic ammonium regeneration and flushing in intertidal sediments of Sado estuary. *Limnol. Oceanogr.* 43 (5), 823–831.
- Rocha, C., 2008. Sandy sediments as active biogeochemical reactors: compound cycling in the fast lane. *Aquat. Microb. Ecol.* 53, 119–127.
- Rocha, C., Forster, S., Koning, E., Epping, E., 2005. High-resolution permeability determination and two-dimensional porewater flow in sandy sediment. *Limnol. Oceanogr.-Meth.* 3, 10–23.
- Rocha, C., Ibanhez, J., Leote, C., 2009. Benthic nitrate biogeochemistry affected by tidal modulation of Submarine Groundwater Discharge (SGD) through a sandy beach face, Ria Formosa, Southwestern Iberia. *Mar. Chem.* 115, 43–58.
- Sadat-Noori, M., Maher, D.T., Santos, I.R., 2016. Groundwater discharge as a source of dissolved carbon and greenhouse gases in a subtropical estuary. *Estuar. Coast* 39, 639–656.
- Schöttner, S., Pfitzner, B., Grünke, S., Rasheed, M., Wild, C., Ramette, A., 2011. Drivers of bacterial diversity dynamics in permeable carbonate and silicate coral reef sands from the Red Sea. *Environ. Microbiol.* 13, 1815–1826.
- Seidel, M., Beck, M., Greskowiak, J., Riedel, T., Waska, H., Suryaputra, I.N.A., Schnetger, B., Niggemann, J., Simon, M., Dittmar, T., 2015. Benthic-pelagic coupling of nutrients and dissolved organic matter composition in an intertidal sandy beach. *Mar. Chem.* 176, 150–163.
- Setia, R., Pichu, R., Petra, M., 2013. Effect of exchangeable cation concentration on sorption and desorption of dissolved organic carbon in saline soils. *Sci. Total Environ.* 465, 226–232.
- Shi, H., Zheng, W., Zhang, X., Zhu, M., Ding, D., 2013. Ecological-economic assessment of monoculture and integrated multi-trophic aquaculture in Sanggou Bay of China. *Aquaculture* 410–411, 172–178.
- Sholkovitz, E., Herbold, C., Charette, M., 2003. An automated dye-dilution based seepage meter for the time-series measurement of submarine groundwater discharge. *Limnol. Oceanogr.-Meth.* 1, 16–28.
- Slater, G.F., White, H.K., Eglinton, T.I., Reddy, C.M., 2005. Determination of microbial carbon sources in petroleum contaminated sediments using molecular ¹⁴C analysis. *Environ. Sci. Technol.* 39, 2552–2558.
- Small, C., Nicholls, R., 2003. A global analysis of human settlement in coastal zones. *J. Coastal Res* 3, 584–599.
- Smith, R.W., Bianchi, T.S., Allison, M., Savage, C., Galy, V., 2015. High rates of organic carbon burial in fjord sediments globally. *Nat. Geosci.* 8, 450.
- Stedmon, C.A., Bro, R., 2008. Characterizing dissolved organic matter fluorescence with parallel factor analysis: a tutorial. *Limnol. Oceanogr.-Meth.* 6, 572–579.
- Techkarnjanaruk, S., Goodman, A.E., 1999. Multiple genes involved in chitin degradation from the marine bacterium *Pseudoalteromonas* sp. strain S91. *Microbiology* 145, 925–934.
- Thamdrup, B., Hansen, J.W., Jørgensen, B.B., 1998. Temperature dependence of aerobic respiration in a coastal sediment. *FEMS Microbiol. Ecol.* 25, 189–200.
- Wang, X., Du, J., Ji, T., Wen, T., Liu, S., Zhang, J., 2014. An estimation of nutrient fluxes via submarine groundwater discharge into the Sanggou Bay—a typical multi-species culture ecosystem in China. *Mar. Chem.* 167, 113–122.
- Wu, Y., Zhu, K., Zhang, J., Müller, M., Jiang, S., Mujahid, A., Muhamad, M.F., Sia, E.S.A., 2019. Distribution and degradation of terrestrial organic matter in the sediments of peat-draining rivers, Sarawak, Malaysian Borneo. *Biogeosciences* 16, 4517–4533.
- Yan, Y., Ma, M., Liu, X., Ma, W., Li, M., Yan, L., 2017. Effect of biochar on anaerobic degradation of pentabromodiphenyl ether (BDE-99) by archaea during natural groundwater recharge with treated municipal wastewater. *Int. Biodeterior. Biodegradation* 124, 119–127.
- Yang, H., Zhou, Y., Mao, Y., Li, X., Liu, Y., Zhang, F., 2005. Growth characters and photosynthetic capacity of *Gracilaria lemaneiformis* as a biofilter in a shellfish farming area in Sanggou Bay, China. *J. Appl. Phycol.* 17, 199–206.
- Yu, T., Wu, W., Liang, W., Lever, M.A., Hinrichs, K.U., Wang, F., 2018. Growth of sedimentary *Bathyarchaeota* on lignin as an energy source. *PNAS* 115, 6022–6027.
- Yuan, M., Zhang, C., Jiang, Z., Guo, S., Sun, J., 2014. Seasonal variations in phytoplankton community structure in the Sanggou, Ailian, and Lidao Bays. *J. Ocean U. China* 13, 1012–1024.
- Zhang, Y., van Dijk, M.A., Liu, M., Zhu, G., Qin, B., 2009. The contribution of phytoplankton degradation to chromophoric dissolved organic matter (CDOM) in eutrophic shallow lakes: field and experimental evidence. *Water Res.* 43, 4685–4697.
- Zhu, X., Zhang, R., Liu, S., Wu, Y., Jiang, Z., Zhang, J., 2017. Seasonal distribution of dissolved iron in the surface water of Sanggou Bay, a typical aquaculture area in China. *Mar. Chem.* 189, 1–9.